Biomedical Signal Processing and Control 48 (2019) 189–196

Contents lists available at ScienceDirect

Biomedical Signal Processing and Control

journal homepage: www.elsevier.com/locate/bspc

A new approach for medical image enhancement based on luminance-level modulation and gradient modulation

Chenyi Zhao[a,1], Zeqi Wang[a,1], Huanyu Li[a], Xiaoyang Wu[a], Shuang Qiao[a,*], Jianing Sun[b,*]

[a] School of Physics, Northeast Normal University, Changchun 130024, China
[b] School of Mathematics & Statistics, Northeast Normal University, Changchun 130024, China

ARTICLE INFO

Article history:
Received 4 February 2018
Received in revised form
17 September 2018
Accepted 6 October 2018
Available online 29 October 2018

Keywords:
Luminance-level modulation
Gradient modulation
Medical images
Image enhancement

ABSTRACT

Medical images play a significant role in modern diagnosis but often suffer from non-uniformity and low-luminance, which always affects the results of diagnosis and even leads to misdiagnosis in real applications. To obtain a clear and accurate view of the medical images, a new method based on luminance-level modulation and gradient modulation (LM&GM) is proposed in this paper. LM&GM is a two-stage approach that, first, increases the visual perception using the luminance-level modulation (LM) operation by compressing the range of luminance levels of the input image, and second, uses the gradient modulation (GM) operation to enhance the details of the previous step result. Experimental results on CT images, X-ray images and MRI images from medical image datasets and quantitative analyses by structural similarity index measurement (SSIM), average gradient (AG), relative enhancement in contrast (REC) and information entropy (IE) demonstrate that the results of the proposed method are competitive and overwhelm those of the existing methods.

1. Introduction

Medical imaging is one of the most widely used techniques for diagnosis, interpretation, and monitoring of disease associated with underlying tissues in the human body [1,2]. The suitability of each medical imaging modality is highly dependent upon the tissue that is to be imaged. In general, X-rays are the most commonly used imaging modality for high-density tissues, such as bones, while magnetic resonance imaging (MRI) and computed tomography (CT) are always used for lower density tissues in the human body. However, due to the restrictions of several factors such as system cost and the inherent properties of the medical imaging, the obtained images always have the properties of low contrast, inadequate brightness, and complex noise. Contrast enhancement of medical images is a very practical and promising means to improve image quality and can increase the accuracy and efficiency in real medical applications [3]. A large number of methods have been proposed to improve the quality of medical images, such as details detection, contrast enhancement, and gray-level transformation [4–6].

Wavelet transform and further developed techniques play an important role in medical image processing such as compression [7], segmentation [8], enhancement, etc. Ref [9]. introduced a medical image resolution enhancement method based on dual-tree complex wavelet transform, nonlocal means filter, and singular value decomposition (DTCWT-NLM-SVD). The dual-tree complex wavelet transform was used to obtain high-frequency subbands, which were used for obtaining the enhanced image combined with the input low-resolution image. An NLM filter was used to weaken the artifacts produced by DTCWT, and SVD was used to enhance the contrast of the image. DTCWT-NLM-SVD achieved the effective result and avoided artifacts simultaneously; but had long-time costs because of complex computation structure. Ref [10]. put forward a graph structure of model images that first adopted wavelet filtering to obtain sparser representations of magnetic resonance images, and then improved the reconstruction performance. This method was consistent with fully sampled images in terms of image intensities and details; but brought about long computation time due to redundancy.

Total variation (TV) methods are one kind of traditional image enhancement methods and are also widely used in medical image processing. A total generalized variation (TGV) was introduced in [11], which suggested the second derivative of the image was further improved versus of the conventional TV, which used the first derivative. This method could preserve the sharp edges of the images effectively but might cause unexpected halos and artifacts. S. J. Liu et al. [12] proposed a joint constraint in the TV framework (JCTV) to model both local sparse and nonlocal similarity of the patch. The image patch was utilized as the unit to improve

* Corresponding authors.
E-mail addresses: qiaos810@nenu.edu.cn (S. Qiao), sunjn118@nenu.edu.cn (J. Sun).
[1] These authors contribute equally to this work.

https://doi.org/10.1016/j.bspc.2018.10.008
1746-8094/

the adaptability of TV norm and the linear minimum mean square error was used to improve the reconstruction performance. This method overcame the staircase effects but omitted the isotropic TV due to the difficulty in decomposing TV-norm in the anisotropic version. Ref [13]. proposed a novel total variation-based $\ell 0$ minimization (TV-$\ell 0$) model for base and detail decomposition. The TV-$\ell 0$ method adopted dynamic range modification in the base layer and detail magnification in the detail layer. The method enhanced the details of images but brought halos and artifacts.

Histogram equalization (HE)-related methods are also useful for image enhancement. Global histogram equalization (GHE) [14] was a straightforward method to enhance the informative regions and the most-frequent gray levels where the most detail information occurred in the image. However, GHE might bring about over-enhancement of the greatest frequent gray levels. A novel average intensity replacement adaptive histogram equalization (AIR-AHE) for MRI image contrast enhancement was proposed in Ref. [15], which consisted of partial contrast stretching, contrast enhancement, window sliding neighborhood operation and new pixel centroid replacement. This method could effectively enhance potential white matte hyper-intensities (WMHs) of MRI images to classify the most possibly correct WMHs. However, the computational time of this method was long due to the iteration operation. Ref [16]. proposed a two-dimensional histogram equalization method (2DHE) for image contrast enhancement. 2DHE was based on histogram equalization and utilized contextual information around each pixel to enhance the contrast of the input image. 2DHE could increase brightness but may also be invalid in revealing complete global information and details.

Other types of contrast enhancement methods have also been adopted for enhancing medical images. Ref. [17] proposed a local and global gray-level S-curve transformation (LGS-Curve). This method applied gray-level S-curve transformation technique locally in medical images obtained from various modalities and enhanced the contrast by increasing the difference between the maximum and minimum gray levels in an image. However, the LGS-Curve method reduced the clarity of small details and caused block effects. Histogram-modified local contrast enhancement (HMLCE) was proposed in [18] to adjust the levels of contrast enhancement, which in turn gave the resultant image a strong contrast and improved the local details present in the original image for a more relevant interpretation. This method incorporated two-stage processing, both histogram modifications and a local contrast enhancement technique, but caused significant halos and artifacts.

The aforementioned methods may work well for some images, such as 8-bit images in the range of luminance levels of 0–255 [19,20]. However, in real applications, the situations of medical images are always complex, especially those that belong to the high dynamic range, because these images are stored in DICOM format. Digital imaging and communications in medicine (DICOM), which is a standard format for medical image storage and communication, is widely used in the field of medical radiation diagnostic [21,22]. The images in DICOM format include 8-bit images and high dynamic range (HDR) images, the familiar types of which are 12-bit images with 4096 luminance levels and 16-bit images with 65,536 luminance levels. Due to the specific characteristics of the imaging environment and principles, the DICOM images always possess the peculiarities of nonuniform luminance levels of pixels and low contrast. The above methods are not completely valid for these high dynamic range images.

In order to obtain a generally applicable enhancement method for DICOM format medical images, a new contrast and details enhancement method based on luminance-level modulation and gradient modulation (LM&GM) is presented in this paper. The LM operation is applied to compress luminance-level range to obtain a better visual quality by protecting the difference between the luminance levels, and GM operation uses an improved fast local Laplacian filters to enhance the details of the image. The experimental results show that LM&GM can improve contrast and enhance details on the visual effects and avoid staircase artifacts when simultaneously compared with the state-of-the-art methods. The objective evaluation and computational time comparison also show the desirable enhancement performance of LM&GM superior to the other methods.

2. Materials and methods

2.1. State-of-the-art method

Local Laplacian filters (LLFs) which were first proposed in Ref. [23] by Paris et al., can achieve high-quality enhancement results by setting a wide range of parameters. However, the speed of these filters was quite slow despite adopting heuristic approximation to reduce the runtime. Fast local Laplacian filters (FLLFs), which are regarded as the accelerated pattern of LLFs by designing a theoretically grounded subsampling, were proposed by Mathieu Aubry for the first time [24]. FLLFs have been widely used in the field of natural images enhancement. The process of FLLFs is shown below:

$$L_\ell(\boldsymbol{O}) = (1-\kappa)L_\ell(r_j(\boldsymbol{I})) + \kappa L_\ell(r_{j+1}(\boldsymbol{I})) \tag{1}$$

where j is a condition such that $\gamma_j \le g \le \gamma_{j+1}$ and the coefficients are interpolated by the precomputed pyramids j and $j+1$. $g = G_\ell(\boldsymbol{I})(x, y)$ is the coefficient of the Gaussian pyramid at level ℓ and position (x, y). The remapping function $r_j(i)$ for $g = \gamma_j$ at sampling point γ_j is sampled as sparsely as possible without losing accuracy. $\{L_\ell(r_j(\boldsymbol{I}))\}$ is a set of precomputed pyramids at level ℓ and κ is calculated by $g = (1-\kappa)\gamma_j + \kappa\gamma_{j+1}$. The remapping function $r_j(i)$ is shown as below:

$$r_j(i) = g + sign(i-g)t(\left|i-g\right|) \tag{2}$$

where $t(x) = c_M^{-1}(c_I(x))$, where $c(\cdot)$ is the cumulative distribution function (CDF) that is calculated by the probability density function (PDF) [25]

$$CDF(i) = \sum_{k=0}^{i} PDF(k) \tag{3}$$

where the PDF is the probability density of each luminance-level in an image, and it can be calculated by:

$$PDF(i) = \frac{n(i)}{H \times W} \tag{4}$$

where $n(i)$ is the number of pixels at luminance level i and $H \times W$ is the size of the image.

2.2. Description of the proposed method

In order to shrink the range of luminance levels of the input image, enhance the visual quality and protect the effective information of the original image, a luminance-level modulation (LM) operation is proposed in this part. Consider an input image $\boldsymbol{V} = \left\{v(m,n) | 1 \le m \le H, 1 \le n \le W\right\}$ with size $H \times W$ and a luminance-level set of $[v_l, v_u]$, where $v(m,n) \in [v_l, v_u]$. The luminance levels of the enhanced image $\boldsymbol{O_{LM}}$ can be compressed into the interval $[o_l, o_u]$, where $\boldsymbol{O_{LM}} = \left\{o(m,n) | 1 \le m \le H, 1 \le n \le W\right\}$, $o(m,n) \in [o_l, o_u]$ and $o_u < v_u$. The LM operation takes into account every luminance level of the input image, and restrains the luminance levels that have a large difference with other luminance levels into a suitable range using mapping. Let $\mathbf{V} = \{v_1, v_2, \ldots, v_N\}$ and $\mathbf{O} = \{o_1, o_2, \ldots, o_N\}$ be the sorted set of N distinct luminance levels of the input image $\boldsymbol{V}$ and output image $\boldsymbol{O_{LM}}$, where $v_1 = v_l <$

$v_2 < \ldots < v_N = v_u$ and $o_1 = o_l < o_2 < \ldots < o_N = o_u$. The mapping is defined as:

$$o_i = \varphi(v_i) = v_i + \omega f(i) \tag{5}$$

where $i = 1, 2, \ldots N$ and ω is a parameter for modulating the compression degree of the luminance levels. Using Eq. (5), each luminance-level of the input image $\boldsymbol{V}$ is transformed to a corresponding output luminance-level to create an enhanced output image $\boldsymbol{O_{LM}}$. In detail, $f(i)$ is defined as:

$$f(i) = \begin{cases} \sum_{j=1}^{i-1} (g_j' - g_j), & i > 1, \\ 0, & otherwise. \end{cases} \tag{6}$$

where $g_j \in \mathbf{G_V} = \{g_1, g_2, \ldots g_{N-1}\}$ and $g_j' \in \mathbf{G_{O_{LM}}} = \{g_1', g_2', \ldots g_{N-1}'\}$. $\mathbf{G_V}$ and $\mathbf{G_{O_{LM}}}$ are the set of the differences of each sorted luminance levels and the recalculated differences, respectively. $g_j = v_{j+1} - v_j$, and g_j' is calculated as:

$$g_j' = k + \left[g_j - k\right]^{S[g_j - k]}, withS(x) = \begin{cases} \alpha, & otherwise, \\ 0, & sgn(x) = 1. \end{cases} \tag{7}$$

where $k = \min\{\mathbf{G_V}\} + (\max\{\mathbf{G_V}\} - \min\{\mathbf{G_V}\}) \cdot \beta$. α and β are the parameters that control the compression degree of luminance levels and that determine the starting point at which the luminance levels need to be compressed, respectively.

FLLFs are effective for enhancing natural images; but may fail in medical images' enhancement. To enhance the details and edges of the DICOM format medical images, a gradient modulation (GM) operation based on improved FLLFs with modified remapping function, is adopted after LM operation. The gradient modulation (GM) is calculated as below:

$$\begin{aligned} &\Phi_\ell(\boldsymbol{O_{GM}}) = (1-\kappa) L_\ell(r_j(\boldsymbol{O_{LM}})) + \kappa L_\ell(r_{j+1}(\boldsymbol{O_{LM}})), \\ &withr_j(i) = g + sgn\left(\exp(-\frac{(i-\gamma_j)^2}{2})\right) t\left(\exp(-\frac{(i-\gamma_j)^2}{2})\right). \end{aligned} \tag{8}$$

where $t(x) = c_{G(M)}^{-1}\left(c_{G(I)}(x)\right)$, $G(M)$ and $G(I)$ are the gradient of the model function and the input image, respectively. $\boldsymbol{O_{LM}}$ is the resulting image of luminance-level modulation and $c(\cdot)$ is the cumulative distribution function calculated by Eq. (3). The output result $\boldsymbol{O_{final}}$ is obtained by collapsing $\Phi(\boldsymbol{O_{GM}})$:

$$\boldsymbol{O_{final}} = \Phi^{-1}(\boldsymbol{O_{GM}}) \tag{9}$$

2.3. Evaluation criteria

Four objective evaluation criteria are utilized to compare the performance of the proposed method against other methods. The criteria are the structural similarity index metric (SSIM), the average gradient (AG), the relative enhancement in contrast (REC) and the information entropy (IE).

SSIM [26] is an index measuring the similarity of the original image x and processed image y, calculated by:

$$SSIM(x,y) = \frac{\left(2\mu_x\mu_y + c_1\right)\left(2\sigma_{xy} + c_2\right)}{\left(\mu_x^2 + \mu_y^2 + c_1\right)\left(\sigma_x^2 + \sigma_y^2 + c_2\right)} \tag{10}$$

where μ_x, μ_y are the average of x and y, respectively; σ_x^2, σ_y^2 and σ_{xy} are the variances and the covariance, respectively. $c_1 = (k_1 L)^2$ and $c_2 = (k_2 L)^2$ are two constants where $k_1 = 0.01$ and $k_2 = 0.03$, and L is the dynamic range of the pixel-value.

AG measures the gradient magnitude of an image and takes the variation of each of the adjacent pixels into account. AG is given as follows:

$$AG = \frac{1}{(H-1)(W-1)} \sum_x \sum_y \frac{\left|G(x,y)\right|}{\sqrt{2}} \tag{11}$$

where $H \times W$ is the size of the image and $G(\bullet)$ is the gradient vector of the image.

REC [14] represents the ratio of the contrast between the input image and the enhanced image. The formula for REC is

$$REC = \frac{C_{processed}}{C_{original}} \tag{12}$$

where C is the average contrast of all 3×3 blocks units. $C_{original}$ and $C_{processed}$ are the contrast of the input image and the processed image, respectively. The REC value of the original image is 1.

IE is an important factor that evaluates the quality of the information in an image. The formula of IE is given by:

$$H(\mathbf{Z}) = -\sum_{z \in \mathbf{Z}} P(z) \log(P(z)) \tag{13}$$

where $\mathbf{Z}$ represents the set of image pixel values, z is the pixel of the image and $P(z)$ represents the probability one pixel value appears.

3. Experiments

3.1. Selection of parameters

The function of α and β are controlling the compression degree of luminance levels and determining the starting point at which the luminance levels need to be compressed, respectively. From (5)-(7) in Section 2.2,

$$\lim_{\alpha \to 1} S(x) \approx 1 \Rightarrow g_j' \approx g_j \Rightarrow f(i) \approx 0 \Rightarrow o_i \approx v_i \Rightarrow \boldsymbol{O_{LM}} \approx \boldsymbol{I_{in}} \tag{14}$$

$$\lim_{\beta \to 1} k \approx \max\{\mathbf{G_v}\} \Rightarrow g_j - k \le 0 \Rightarrow S(x) = 1 \Rightarrow \boldsymbol{O_{LM}} \approx \boldsymbol{I_{in}} \tag{15}$$

Eqs. (14) and (15) represent the series of connected results for the condition that $\alpha = 1$ and $\beta = 1$. When $\alpha = 1$, the recalculated difference g_j' is equal to g_j, so the function $f(i) = 0$, meaning that the compressed image is the same as the input image. When $\beta = 1$, the threshold k is equal to the maximum of the luminance levels' difference from the original image, which leads to the compare function $S(x) = 1$; therefore, the result by (15) is the same as the result by (14). The value of k is more than or equal to the minimum of $\mathbf{G_V}$, and β is usually more than zero. Generally, the range of α and β is 0-1.

The processed results of LM for different values of α and β are shown in Figs. 1 and 2, from which one can see that the enhanced result becomes better visually as α gets smaller when $\beta = 0.01$, and the same trend is seen as β changes when $\alpha = 0.5$. From the comparison of Fig. 1 (d) and (e), the results are similar visually for $\alpha = 0.5$ and $\alpha = 0.1$, whereas, theoretically, the too small value of α may cause over-compression and affect the quality of the image, as α is used for compressing the luminance levels range. Consequently, the parameters α and β are set to be 0.5 and 0.01, respectively.

Figs. 3 and 4 show the original images, the processed results by LM, and the corresponding histograms of luminance-level distribution. In the experiment, the parameters ω, α and β are set to be 1, 0.5, and 0.01, respectively. Figs. 3(a) and 4 (a) show the images and global luminance-level histograms, in which the horizontal and the vertical axes represent the luminance levels of the images and their corresponding probability density, respectively. The LM operation can keep the overall trend of probability density

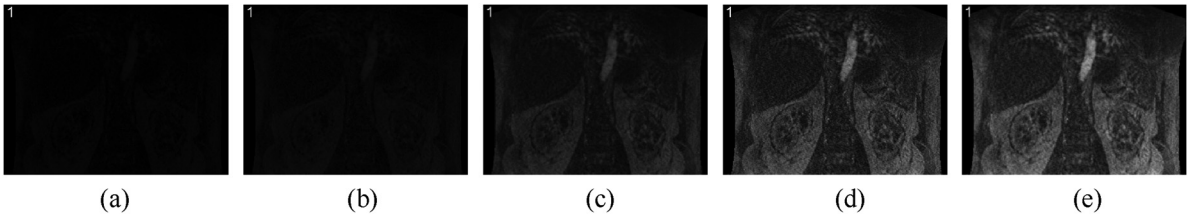

Fig. 1. The original breast MRI image and images processed by LM for different values of α with $\beta = 0.01$: (a) Original image; (b) Enhanced result for $\alpha = 0.9$; (c) Enhanced result for $\alpha = 0.7$; (d) Enhanced result for $\alpha = 0.5$; (e) Enhanced result for $\alpha = 0.1$.

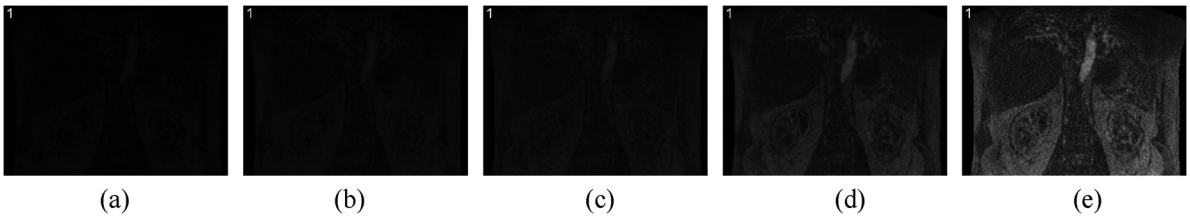

Fig. 2. The original breast MRI image and images processed by LM for different values of β with $\alpha = 0.5$: (a) Original image; (b) Enhanced result for $\beta = 0.5$; (c) Enhanced result for $\beta = 0.3$; (d) Enhanced result for $\beta = 0.1$; (e) Enhanced result for $\beta = 0.01$.

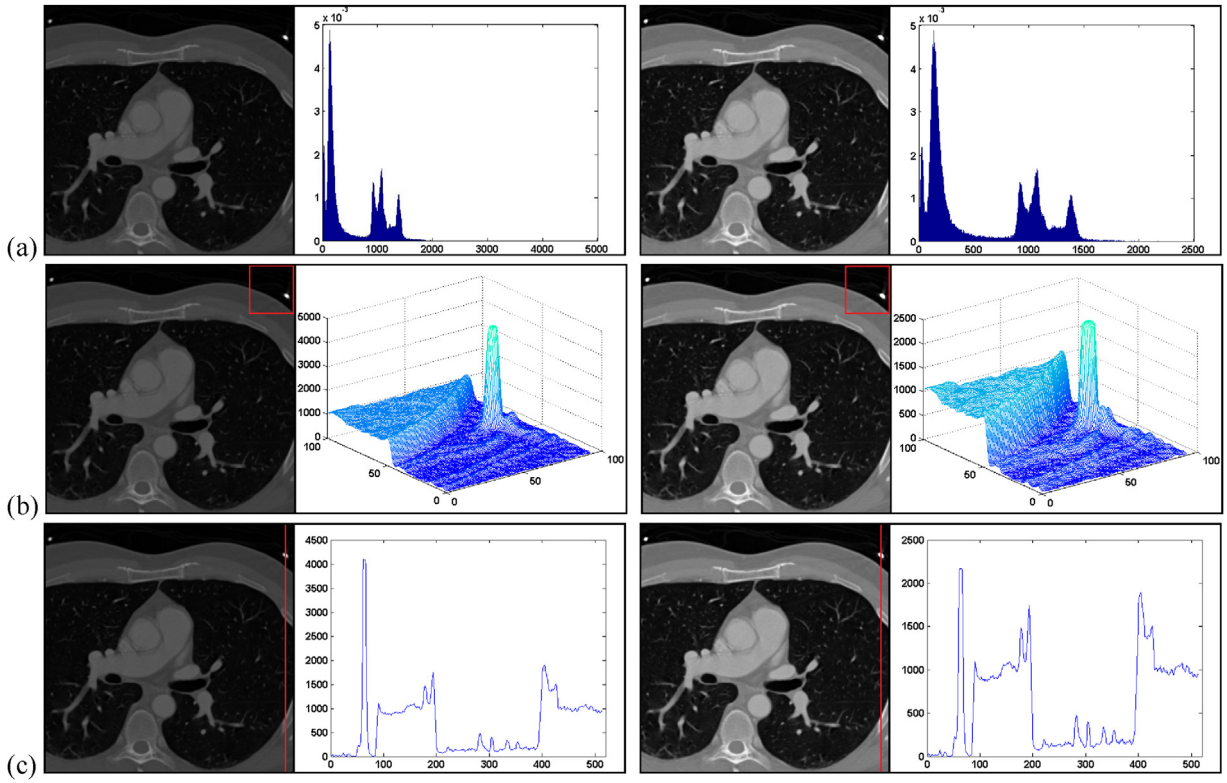

Fig. 3. The original heart CT images, processed results and corresponding histograms.

unchanged before and after processing. We crop the square area of the heart CT image and the buttock MRI image and show the relevant three-dimensional histograms in Figs. 3(b) and 4 (b). Further, the line-scan data, represented as a red line, are shown in Figs. 3(c) and 4 (c); specifically, the horizontal and vertical axes represent the location and the corresponding luminance-level. The comparison results show that the LM operation can enhance the contrast of medical images, while simultaneously preserving the difference between different luminance levels of the images.

3.2. Description of results

In this section, some experiments on the real CT images and MRI images from medical images database [27] are taken to investigate the performance of our proposed method LM&GM. LM&GM is compared with the related state-of-the-art methods: 2DHE [16], HMLCE [18], LGS-Curve [17] and FLLFs [24]. The four objective image quality criteria described in Section 2.3 are used. In the experiments, the parameters are set as $\omega = 1$, $\alpha = 0.5$, $\beta = 0.01$, and $j_{\max} = 10$. All the above methods are performed on a PC

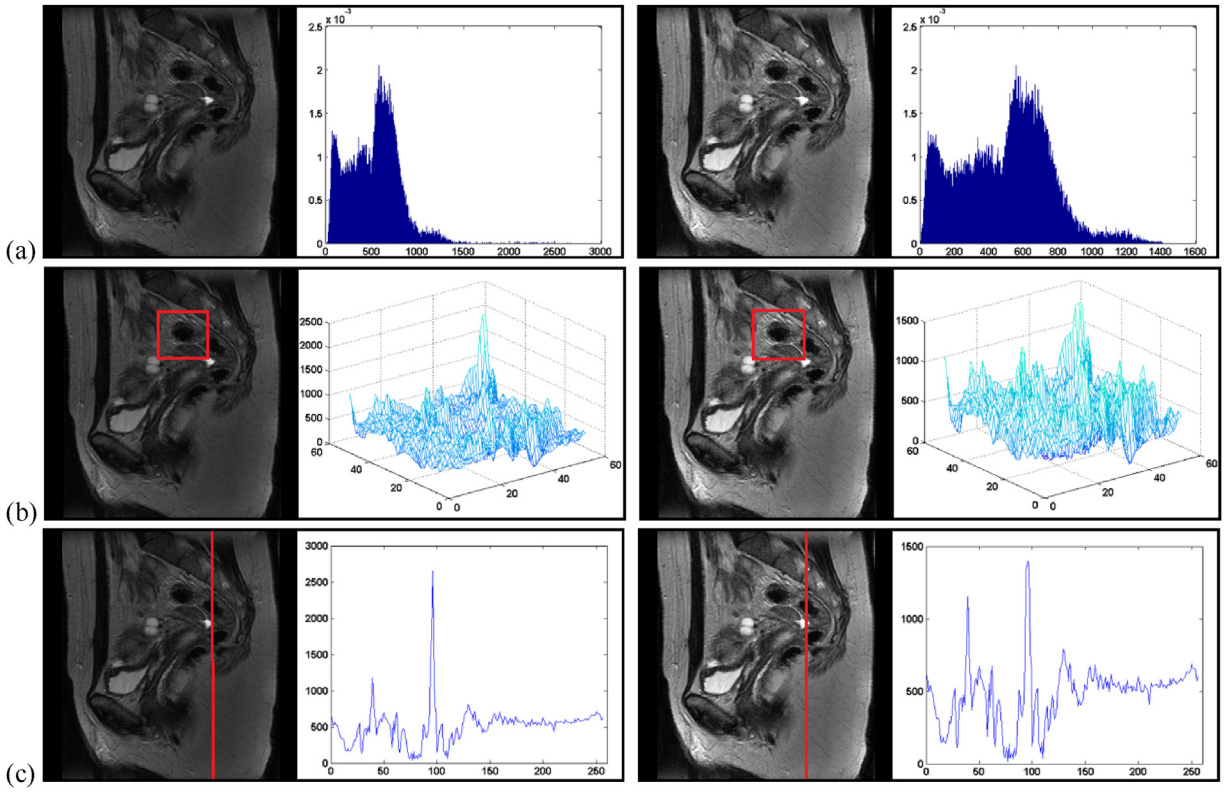

Fig. 4. The original buttock MRI images, processed results and corresponding histograms.

equipped with Intel Core i5-4590 CPU 3.3 GHz, memory 4GB, and the methods are coded in MATLAB software on Windows 7 32-bit.

The enhancement results of a chest CT image with size 400×512, a diastolic heart CT with size 512×512, and a mammogram with size 2294×1914 are shown in Fig. 5. One heart MRI image with size 256×244 and a buttock MRI image with size 440×440 and the enhanced results are shown in Figs. 6 and 7, respectively. From the experimental results we can conclude that 2DHE can improve the brightness but may also be invalid in revealing complete global information and details. HMLCE can slightly enhance the details of the image but causes significant halos and artifacts. The results of LGS-Curve are overly bright and cannot adequately show the whole contents of the enhanced image. The results of FLLFs are clear but lack of some textures and smooth areas that presented in the original image. As seen from Figs. 5(f), 6 (f) and 7 (f), the results of LM&GM can not only increase the contrast of the images but can also enhance the details of the images, which show better visual assessment than the other methods.

Accuracy measurement is necessary for further comparison between the proposed method and existing methods. The evaluation criteria of SSIM, AG, REC, and IE are employed to compare the enhancement effects of these methods. Table 1 records the values of SSIM, AG, REC, and IE of the enhanced images of each enhancement

Table 1
The values of the evaluation criteria by different enhancement methods for the medical images.

Images	Metrics	Results of different Methods					
		Original	2DHE	HMLCE	LGS-Curve	FLLFs	LM&GM
Chest CT	SSIM	1.0000	0.9877	0.8698	0.6254	0.9978	0.9991
	REC	1.0000	1.5024	1.0387	1.4764	1.3756	1.6267
	AG	5.0068	7.5583	5.1595	7.2330	7.1105	8.4538
	IE	6.4985	3.4427	6.8412	6.3131	5.8911	7.3231
Heart CT	SSIM	1.0000	0.9961	0.4438	0.4882	0.9978	0.9970
	REC	1.0000	1.4535	1.1308	1.5232	1.2882	1.4345
	AG	51.2485	63.1354	61.6046	51.1136	53.0349	113.3996
	IE	4.4751	4.6736	5.7705	5.0259	3.8870	6.8880
Mammograms	SSIM	1.0000	0.9884	0.7604	0.4718	0.9966	0.9973
	REC	1.0000	1.2123	1.4941	1.1753	1.0080	1.2289
	AG	5.3445	9.4225	5.6737	6.8010	6.0120	24.4777
	IE	0.6773	2.6399	4.4260	4.1436	0.3097	4.7170
Cardiac MRI	SSIM	1.0000	0.9937	0.3364	0.6754	0.9978	0.9991
	REC	1.0000	2.9037	1.0276	4.1740	2.7076	4.4026
	AG	16.3090	47.5390	16.3294	19.3090	20.0845	49.7931
	IE	7.1782	5.0597	6.8321	7.2028	7.0565	7.7078
Buttock MRI	SSIM	1.0000	0.9882	0.6407	0.4892	0.9977	0.9945
	REC	1.0000	1.4677	1.2101	1.6621	1.3930	1.6758
	AG	149.8942	221.3285	149.7068	175.3217	156.1062	247.2245
	IE	2.1809	2.5480	6.2573	6.5593	1.7135	7.0504

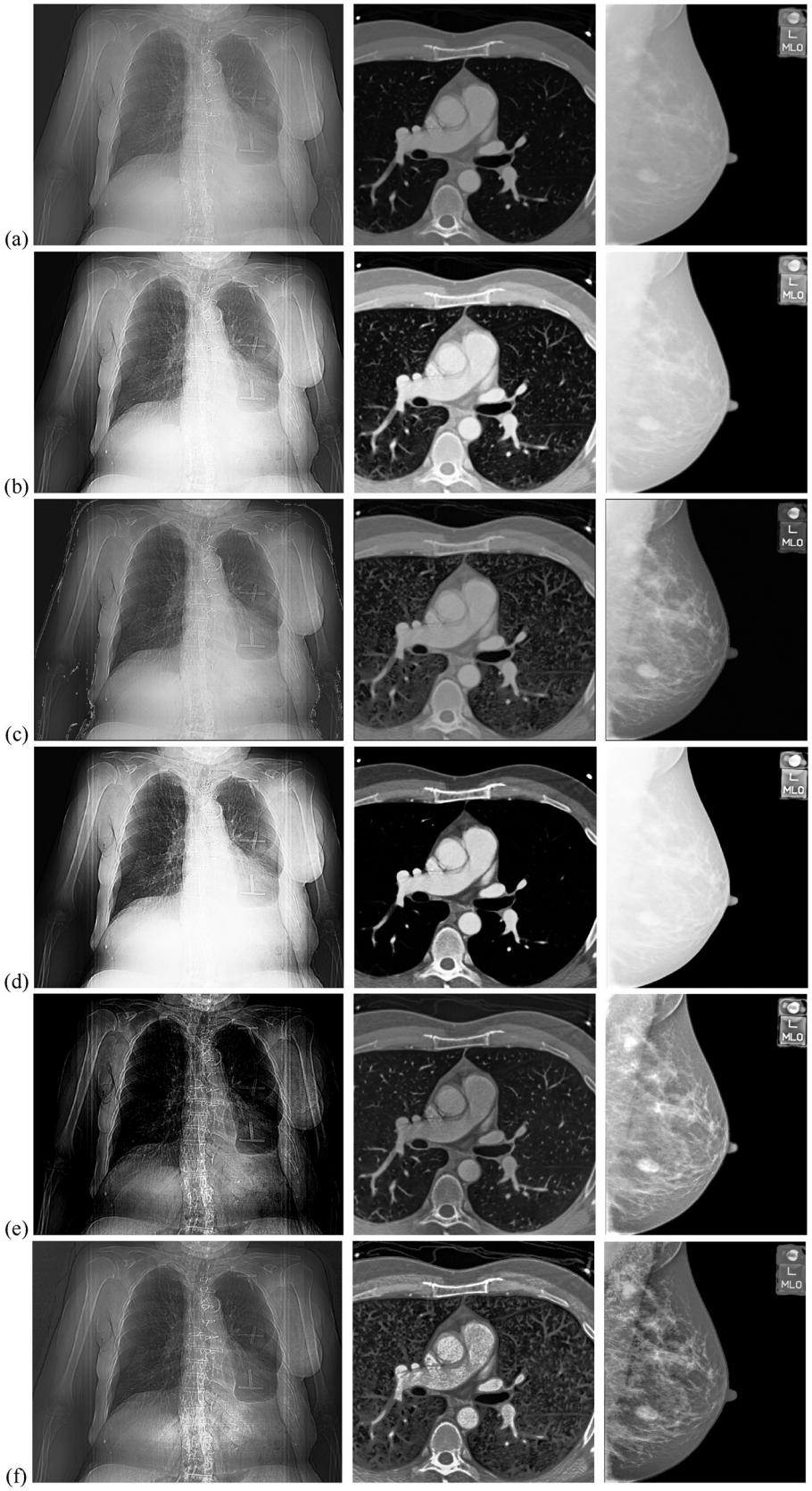

Fig. 5. Enhancement results of real high-bit DICOM format images: (a) Original images; (b) Results of 2DHE; (c) Results of HMLCE; (d) Results of LGS-Curve; (e) Results of FLLFs; (f) Results of LM&GM.

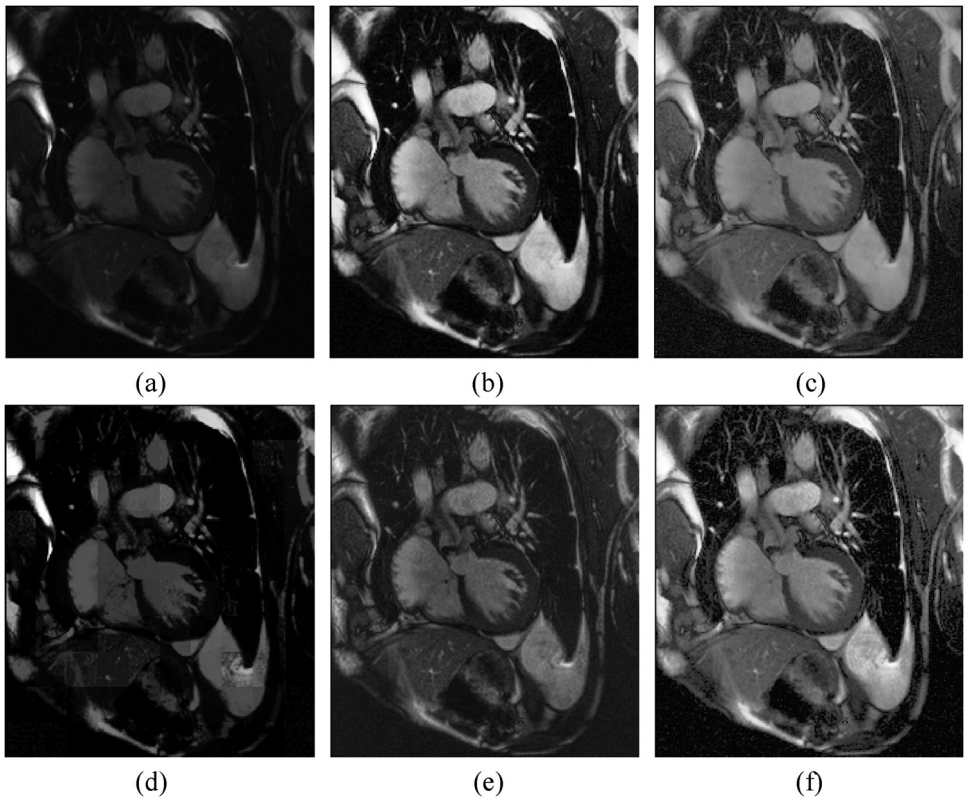

Fig. 6. Enhancement results of real high-bit DICOM format heart MRI image: (a) Original image; (b) Result of 2DHE; (c) Result of HLMCE; (d) Result of LGS-Curve; (e) Result of FLLFs; (f) Result of LM&GM.

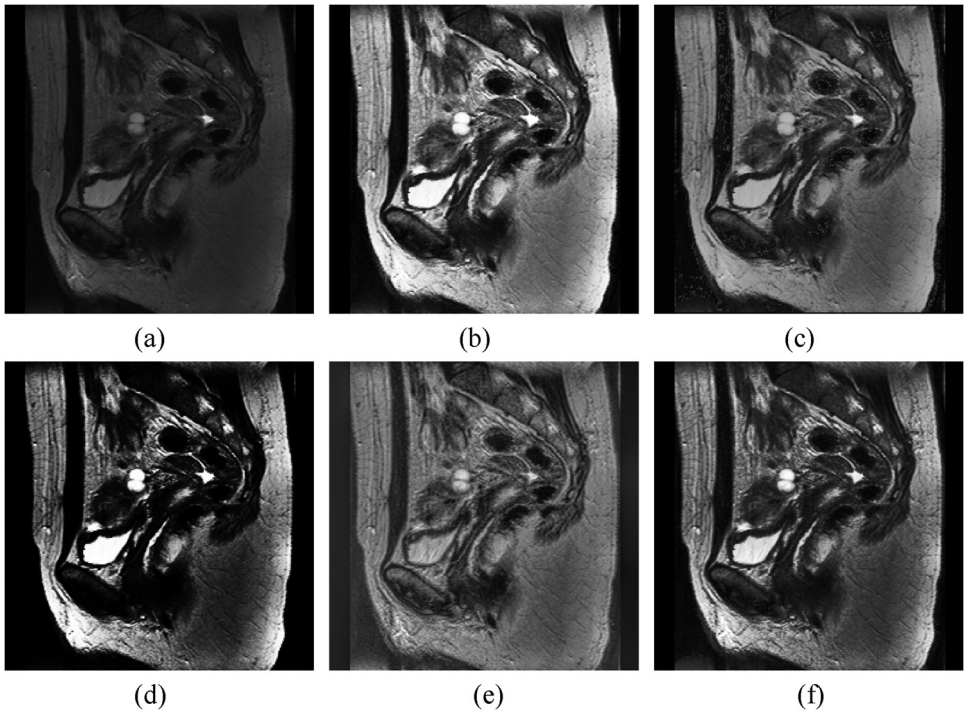

Fig. 7. Enhancement results of real high-bit DICOM format buttock MRI image: (a) Original image; (b) Result of 2DHE; (c) Result of HLMCE; (d) Result of LGS-Curve; (e) Result of FLLFs; (f) Result of LM&GM.

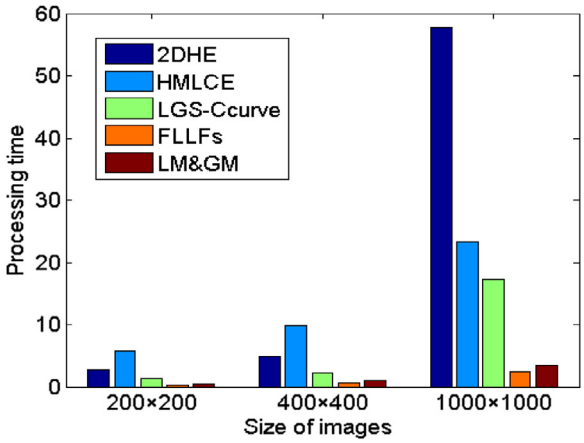

Fig. 8. CPU time comparison of 2DHE, HLMCE, LGS-Curve, FLLFs and LM&GM.

methods. The higher values of SSIM, AG, and IE illustrate the better capability of LM&GM for enhancing the details, textures, and contrast in comparison with the other methods. The RECs of the results show that LM&GM also has a beneficial effect on medical image enhancement.

Fig. 8 shows the computational time of 2DHE, HLMCE, LGS-Curve, FLLFs and the proposed LM&GM. For ensuring reliability, all the time data are obtained by taking the average of ten times the experimental results. The LM&GM method has a better time-consuming performance than 2DHE, HLMCE and LGS-Curve. Though the time of LM&GM is slightly longer than that of the existing FLLFs, the enhanced images of LM&GM are better than that of the FLLFs in terms of both the visual assessment and quantitative evaluation.

4. Conclusion

A novel medical image enhancement method based on luminance-level modulation and gradient modulation is proposed in this paper. The main contributions of this paper include two aspects: first, the proposal of a novel luminance-level modulation (LM) operation, which could shrink the dynamic range of luminance levels instead of clipping the fraction of high-brightness by a predefined threshold, and second, the gradient modulation (GM) operation adopted improved fast local Laplacian filter is used to enhance the details and textures of the images further. The performance of the proposed method was compared with popular enhancement methods such as 2DHE, HMLCE, LGS-Curve and FLLFs, both qualitatively and objectively, which illustrates that LM&GM is superior to the other methods in enhancing details, increasing contrast and avoiding artifacts and halos. The time comparisons between different methods also demonstrate the advantages of stability and practicability of LM&GM.

Acknowledgments

This work is supported by National Key Scientific Instrument and Equipment Development Projects (Grant no. 2013YQ040861), National Natural Science Foundation of China (Grant no. 11275046), National Natural Science Foundation of China (Grant no. 11505026), Opening Project of Science and Technology on Reliability Physics and Application Technology of Electronic Component Laboratory (ZHD201701).

References

[1] R. Kumar, S. Basu, D. Torigian, Role of modern imaging techniques for diagnosis of infection in the era of 18F-Fluorodeoxyglucose positron emission tomography, Clin. Microbiol. Rev. 21 (1) (2008) 209–224.
[2] A.P. James, B.V. Dasarathy, Medical image fusion: a survey of the state of the art, Inform. Fusion 19 (3) (2014) 4–19.
[3] B.C. Patel, G.R. Slinha, Gray level clustering and contrast enhancement (GLC-CE) of mammographic breast cancer images, Csi Trans. Ict. 2 (4) (2015) 279–286.
[4] J. Shi, Z. Shan, Image resolution enhancement using statistical estimation in wavelet domain, Biomed. Signal Process. Control. 7 (6) (2012) 571–578.
[5] T. Doshi, J. Soraghan, L. Petropoulakis, Automatic pharynx and larynx cancer segmentation framework (PLCSF) on contrast enhanced MR images, Biomed. Signal Process. Control 33 (2017) 178–188.
[6] S. Anand, R.S.S. Kumari, S. Jeeva, Directionlet transform based sharpening and enhancement of mammographic X-ray images, Biomed. Signal Process. Control 8 (2013) 391–399.
[7] T. Bruylants, A. Munteanu, P. Schelkens, Wavelet based volumetric medical image compression, Signal Process Image Commun. 31 (36) (2015) 112–133.
[8] J.V. Soares, J. Leandro, Retinal vessel segmentation using the 2-D Gabor wavelet and supervised classification, IEEE Trans. Med. Imaging 25 (9) (2006) 1196–1204.
[9] M.Z. Iqbaletal, Dual-tree complex wavelet transform and SVD based medical image resolution enhancement, Signal Process. 105 (12) (2014) 430–437.
[10] Z. Lai, X. Qu, Y. Liu, Image reconstruction of compressed sensing MRI using graph-based redundant wavelet transform, Med. Image Anal. 21 (6) (2016) 27–93.
[11] F. Knoll, K. Bredies, T. Pock, Second order total generalized variation (TGV) for MRI, Magn. Reson. Med. 65 (2) (2011) 480–491.
[12] S. Liu, J. Cao, H. Liu, MRI reconstruction using a joint constraint in patch-based total variational framework, J. Vis. Commun. Image Representat. 46 (2017) 150–164.
[13] S. Qiao, G.Y. Bai, J.N. Sun, Digital neutron image enhancement based on total variation- based $\ell 0$ minimization, Nuclear Instrum. Methods Phys. Res. A 806 (11) (2016) 154–158.
[14] J. Joseph, R. Periyasamy, A fully customized enhancement scheme for controlling brightness error and contrast in magnetic resonance images, Biomed. Signal Process. Control 39 (2018) 271–283.
[15] I.S. Isa, S.N. Sulaiman, M. Mustapha, Automatic contrast enhancement of brain MR images using Average Intensity Replacement based on Adaptive Histogram Equalization (AIR-AHE), Biocybernet. Biomed. Eng. 37 (1) (2017) 24–34.
[16] T. Celik, Two-dimensional histogram equalization and contrast enhancement, Pattern Recognit. 45 (10) (2012) 3810–3824.
[17] A. Gandhamal, S. Talbar, S. Gajre, Local gray level S-curve transformation-a generalized contrast enhancement technique for medical images, Comput. Biol. Med. 83 (2017) 120–133.
[18] M. Sundaram, K. Ramar, N. Arumugam, G. Prabin, Histogram modified local contrast enhancement for mammogram images, Appl. Soft Comput. 11 (8) (2011) 5809–5816.
[19] H.S. Gan, T.T. Swee, A.H.A. Karim, Medical image visual appearance improvement using bihistogram bezier curve contrast enhancement: data from the osteoarthritis initiative, Sci. World J. 2014 (1) (2014), 294104 1-13.
[20] H.S. Gan, T.T. Swee, B.A.K.M. Rafiq, Medical image contrast enhancement using spline concept: data from the osteoarthritis initiative, J. Med. Imag. Health Inform. 4 (4) (2014) 511–520.
[21] K.C. Jr, J.A. Carrno, M.J. Flynn, DICOM and radiology: past, present, and future, J. Am. Coll. Radiol. Jacr 4 (9) (2007) 652–657.
[22] O.S. Pianykh, Digital imaging and communications in medicine (DICOM), J. Nuclear Med. 50 (8) (2012) 1384.
[23] S. Paris, S.W. Hasiniff, J. Kautz, Local Laplacian filters: edge-aware image processing with a Laplacian pyramid, ACM Trans. Graphics 30 (4) (2011) 68.
[24] S. Paris, S.W. Hasinoff, J. Kautz, Fast local laplacian filters: theory and applications, ACM Trans. Graphics 33 (5) (2014) 167.
[25] R.C. Gonzales, R.E. Woods, Digital Image Processing, Prentice Hall, 2002.
[26] Z. Wang, Image quality assessment: from error visibility to structural similarity, IEEE Trans. Image Process. 13 (4) (2004) 600–612.
[27] S. Barre, http://www.barre.nom.fr/medical/samples/index.html.